Sputtering of amorphous silicon nitride irradiated with energetic C60 ions: Preferential sputtering and synergy effect between electronic and collisional sputtering

AUTHOR(S):

Kitayama, T.; Morita, Y.; Nakajima, K.; Narumi, K.; Saitoh, Y.; Matsuda, M.; Sataka, M.; Toulemonde, M.; Kimura, K.

CITATION:

Kitayama, T. ...[et al]. Sputtering of amorphous silicon nitride irradiated with energetic C60 ions: Preferential sputtering and synergy effect between electronic and collisional sputtering. Nuclear Instruments and Methods in Physics Research Section B: Beam Interactions with Materials and Atoms 2015, 365: 490-495

ISSUE DATE:

2015-12-15

URL:

http://hdl.handle.net/2433/207607

Sputtering of amorphous silicon nitride irradiated with energetic C_{60} ions: Preferential sputtering and synergy effect between electronic and collisional sputtering

T. Kitayama[1], Y. Morita[1], K. Nakajima[1], K. Narumi[2], Y. Saitoh[2], M. Matsuda[3], M. Sataka[3], M. Toulemonde[4], and K. Kimura[1, *]

[1]Department of Micro Engineering, Kyoto University, Kyoto 606-8501, Japan

[2]Takasaki Advanced Radiation Research Institute, Japan Atomic Energy Agency, 1233 Watanuki-machi, Takasaki, Gumma 370-1292, Japan

[3]Nuclear Science Research Institute, Japan Atomic Energy Agency, Tokai, Naka, Ibaraki 319-1195, Japan

[4]CIMAP-GANIL (CEA-CNRS-ENSICAEN-Université de Caen Basse Normandie), Bd. H. Becquerel, 14070 Caen, France

[*]e-mail: kimura@kues.kyoto-u.ac.jp

Amorphous silicon nitride films (thickness 30 nm) deposited on Si(001) were irradiated with 30 – 1080 keV C_{60} and 100 MeV Xe ions to fluences ranging from 2×10^{11} to 1×10^{14} ions/cm^2. The composition depth profiles of the irradiated samples were measured using high-resolution Rutherford backscattering spectrometry. The sputtering yields were estimated from the derived composition profiles. Pronounced preferential sputtering of nitrogen was observed in the electronic energy loss regime. In addition, a large synergy effect between the electronic and collisional sputtering was also observed. The sputtering yields were calculated using the unified thermal spike model to understand the observed results. Although the calculated results reproduced the observed total sputtering yields with a lowered sublimation energy, the observed preferential sputtering of nitrogen could not be explained. The present results suggest an additional sputtering mechanism related to the electronic energy loss.

1. INTRODUCTION

When solid surface is bombarded with energetic ions the surface atoms are removed. This is called *sputtering*, which is the basis of many applications, such as sputtering deposition, plasma etching, surface analysis and so on. For the bombardment of low energy ions the sputtering is caused by elastic collisions between the incoming ions and the atoms in the surface layers and closely linked to the nuclear energy loss [1]. On the contrary, for the bombardment of high energy ions, the elastic collision plays a minor role in the sputtering process because the kinetic energy of the high energy ion is deposited almost exclusively to the target electrons. Nevertheless, the surface erosion is observed especially with insulators [2]. This is called *electronic sputtering* and in some cases huge sputtering yields, more than 1000 atoms/ion, were observed. The origin of the electronic sputtering is attributed to the electron-phonon coupling. The energy deposited to the electrons (electronic energy loss) is transferred to the atomic subsystem and this causes large local heating where surface atoms are removed by thermal evaporation. Such a local heating can be described by a so-called inelastic thermal spike (i-TS) model [3], which was originally developed to explain the formation of ion tracks produced by swift heavy ions. Based on the i-TS model, the observed sputtering yields of crystalline and vitreous SiO_2 irradiated with swift heavy ions were well reproduced [4].

Thus, the mechanism of sputtering is well understood in both low and high energy regimes. In the intermediate energy regime, the synergy effect between the collisional and electronic sputtering may play an important role. There is, however, almost no study on the synergy effect in the intermediate energy regime. This is partly because both the collisional and electronic sputtering yields are small in the intermediate energy regime. As a result, notable synergy effect is not expected. This is true for monoatomic ions but is not the case for the cluster ions. For the cluster ions, both the electronic and nuclear energy losses may be large enough to lead to a notable synergy effect in the intermediate energy regime. In this paper, the sputtering yields of amorphous silicon nitride (a-SiN) irradiated with 30 – 1080 keV C_{60} ions are measured to study the synergy effect. Differently from monoatomic ions, both nuclear and electronic energy losses of these C_{60} ions are rather large (~10

keV/nm) in this energy regime.

II. EXPERIMENTAL

A wafer of Si(001) with an a-SiN film (thickness 30 nm) deposited by low pressure chemical vapor deposition (LPCVD) was purchased from Silson Ltd. The nominal density of the a-SiN film is 3 g/cm^3. Beams of 30 - 1080 keV C_{60} ions were produced by the 400-kV ion implanter at JAEA/Takasaki. The a-SiN/Si(001) samples were irradiated with the C_{60} ion beams at normal incidence to fluences from 2×10^{12} to 1×10^{14} ions/cm^2 under a vacuum of 10^{-5} Pa. For comparison, the a-SiN/Si(001) sample was irradiated with 100 MeV Xe ions to a fluence of 4×10^{13} ions/cm^2 at JAEA/Tokai.

After irradiation, the composition depth profiles of the samples were measured using high-resolution Rutherford backscattering spectrometry (RBS) at Kyoto University. The details of the high-resolution RBS measurement were described elsewhere [5]. Briefly, He^+ ions were produced by a Penning ion gauge type ion source and accelerated up to 400 keV by a Cockcroft Walton type accelerator. The He^+ beam was collimated to 2×2 mm^2 and a divergence angle less than 1 mrad by two sets of rectangular shaped slit system and sent to a scattering chamber (base pressure 2×10^{-8} Pa). The beam current was monitored by a beam chopper and the typical beam current was about 50 nA. The He ions scattered from the sample at a scattering angle of 75º were energy analyzed by a 90º sector type magnetic spectrometer and detected by a one-dimensional position sensitive detector (1D-PSD) of 100 mm length (the energy window was 25% of the central energy). The RBS measurements were performed under channeling (<110> and/or <111> axial channeling) and random conditions for each sample. During the random measurement the sample was continuously rotated around the surface normal to avoid undesirable channeling and/or blocking effects.

III. RESULTS

Figure 1 shows an example of the observed RBS spectra. The dashed and solid lines show the random and <111> channeling spectra, respectively, of the pristine a-SiN/Si(001). The plateau seen from ~282 to ~323 keV corresponds to Si signals in the

a-SiN film. Nitrogen signals are seen from ~225 to ~259 keV. There are small peaks at ~273 and ~241 keV, which correspond to oxygen and carbon atoms at the surface. From these spectra composition depth profiles were derived through spectrum simulations. The obtained result is shown by open symbols in Fig. 2. The concentrations of silicon and nitrogen are almost constant in the film, which are 49% and 51% for silicon and nitrogen, respectively, indicating that the film composition is slightly Si-rich compared to the stoichiometric Si_3N_4. The depth scale shown in the upper abscissa was calculated from the stopping power estimated with SRIM2011 [6]. From the width of the trapezoidal nitrogen profile, the thickness of the a-SiN film is estimated to be 30.3 nm, which is in good agreement with the nominal thickness of 30 nm. In addition to silicon and nitrogen, there are carbon atoms of 1×10^{15} atoms/cm^2 on the surface. These carbon atoms are attributed to a thin surface contamination layer consisting of hydrocarbon. Similar amount of surface carbon was also observed for all irradiated samples. There are also oxygen atoms of 3×10^{15} atoms/cm^2 in the surface region, indicating that a thin silicon oxynitride layer (thickness ~1 nm) was formed at the surface.

The sample was also measured after the irradiation of C_{60} ions. Examples of the observed random and <111> channeling spectra for the sample irradiated with 540 keV C_{60} ions to a fluence of 5.2×10^{12} ions/cm^2 are shown by circles and triangles, respectively, in Fig. 1. The composition depth profiles derived from these spectra are shown by solid symbols in Fig. 2. Compared to the results of the pristine sample, the Si and N profiles shift towards the surface by ~6 nm, showing that a part of a-SiN film was removed by sputtering. In addition to the thinning of the a-SiN film, the composition was changed especially in the surface region. The silicon concentration increased and the nitrogen concentration decreased after irradiation, indicating preferential sputtering of nitrogen. The preferential sputtering changed the film composition from the surface down to ~15 nm in this case.

The RBS measurements were also performed for the samples irradiated with C_{60} ions at different energies as well as the sample irradiated with 100 MeV Xe ions and the composition depth profiles were derived. Similarly to the 540 keV C_{60}, the surface composition was changed after irradiation. The thickness of the composition changed layer

increases with increasing energy of C_{60}. For 100 MeV Xe, the composition was changed throughout the film. The amount of each element in the a-SiN film was derived by integrating the observed profile. Figures 3 and 4 show the fluence dependence of the observed amount of Si and N in the a-SiN film. These results were fitted by exponential functions and the fitting results are shown by dashed curves. The partial sputtering yields of silicon, Y_{Si}, and nitrogen, Y_N, were estimated by the slope of these curves at zero fluence. The obtained sputtering yields are summarized in Table 1 together with the electronic and nuclear energy losses calculated using SRIM2011.

IV. DISCUSSION

It is seen from the Table 1 that the nuclear energy loss S_n of 1080 keV C_{60} is smaller than that of 30 keV C_{60}, and the electronic energy loss S_e of 1080 keV C_{60} is smaller than that of 100 MeV Xe. This leads to the following relations because the collisional (electronic) sputtering yield Y_c (Y_e) increases with the nuclear (electronic) energy loss,

$$Y_c(1080\text{keV } C_{60}) < Y_c(30\text{keV } C_{60}) < Y(30\text{keV } C_{60}), \quad (1)$$

and

$$Y_e(1080\text{keV } C_{60}) < Y_e(100\text{ MeV Xe}) < Y(100\text{ MeV Xe}). \quad (2)$$

If there is no synergy effect between the collisional and electronic sputtering, the sputtering yield is given by the sum of the collisional and electronic sputtering yields, *i.e.* $Y = Y_c + Y_e$. Thus, the following relation can be derived from Eqs. (1) and (2),

$$Y(1080\text{keV } C_{60}) < Y(30\text{keV } C_{60}) + Y(100\text{ MeV Xe}). \quad (3)$$

The observed yield Y(1080keV C_{60}) = 4590 is, however, much larger than the sum of Y(30keV C_{60}) = 1200 and Y(100 MeV Xe) = 460. This clearly indicates that there is a strong synergy effect between the collisional and electronic sputtering. It is also noteworthy that the ratio of the observed partial sputtering yields, Y_N/Y_{Si}, ranges from 1.4 to 9. These sputtering yield ratios are much larger than the concentration ratio, 1.04 = 0.51/0.49, showing a remarkable preferential sputtering of nitrogen.

Table 1 also shows the collisional sputtering yields calculated using the SRIM code. In the calculation, the cluster effect was neglected, namely the calculated sputtering yield for

the monoatomic carbon ion of the same velocity was multiplied by 60. The estimated sputtering yields are one to three orders of magnitude smaller than the observed results. Because the present SRIM estimation includes only the ballistic collision-cascade (linear collision cascade) mechanism this indicates that the observed sputtering yields are mainly attributed to the electronic sputtering mechanism and the elastic-collision spike mechanism.

There are several mechanisms proposed for the electronic sputtering, such as Coulomb explosion model [7], multi-exciton model [8], and i-TS model [2, 4]. Among these models, only the i-TS model provides quantitative estimation of the sputtering yield and successfully explained observed sputtering yields [2, 4]. The i-TS model was originally developed to explain the track formation, which describes the temperature evolution of the electronic and atomic subsystems using two heat diffusion equations. Recently, the i-TS model was extended to include the synergy effect between the elastic collision spike and the inelastic thermal spike in the track formation [9]. In the u-TS model, the heat diffusion in time t and space r (radial distance from the ion path) is described by the following differential equations,

$$C_e(T_e)\frac{\partial T_e}{\partial t} = \frac{1}{r}\frac{\partial}{\partial r}\left[rK_e(T_e)\frac{\partial T_e}{\partial r}\right] - g(T_e - T_a) + A(r,v,t), \quad (4)$$

$$C_a(T_a)\frac{\partial T_a}{\partial t} = \frac{1}{r}\frac{\partial}{\partial r}\left[rK_a(T_a)\frac{\partial T_a}{\partial r}\right] + g(T_e - T_a) + B(r,t), \quad (5)$$

where $T_{e,\,a}$, $C_{e,\,a}$ and $K_{e,\,a}$ are the respective temperature, specific heat and thermal conductivity of the electronic and atomic subsystems, g is the electron-phonon coupling constant, $A(r, v, t)$ and $B(r, t)$ are energy inputs into the electronic and atomic subsystems from the electronic and nuclear energy losses, and v is the ion velocity. It is generally assumed that the track core and the shell are produced when the temperature surpasses the boiling energy (E_b) and the melting energy (E_m), respectively [10, 11]. The observed core and shell radii of ion tracks in a-SiN produced by 0.12 – 5 MeV C_{60} ions as well as swift heavy ions such as 420 MeV Au ions were successfully reproduced by the u-TS calculations with E_b = 2.5 eV/atom and E_m = 0.62 eV/atom [12]. The evolutions of atomic and electronic temperatures were calculated using the u-TS model with the same parameter values

used in Ref. 12.

Using the evolution of temperature distribution, $T_a(r, t)$, the evaporation rate Φ_i of i species is given by [13]

$$\Phi_i\left(T_a(r,t)\right) = N_i\sqrt{\frac{k_B T_a(r,t)}{2\pi M_i}}\exp\left(\frac{-U_i}{k_B T_a(r,t)}\right), \tag{6}$$

where k_B is the Boltzmann constant, N_i is the atomic density of i species, M_i is the atomic mass of i species and U_i is the sublimation energy of i species. The sputtering yield can be estimated by integrating the evaporation rate in time t and space r on the surface. Note that this includes the contribution of the elastic-collision spike through $B(r, t)$ and also the synergy effect between the collisional and electronic sputtering through the electron-phonon coupling.

Figure 5 shows the comparison between the observed and calculated total sputtering yields. In the calculation, the sublimation energy U was approximated by the boiling energy E_b (= 2.5 eV [12]) for both Si and N. The calculated sputtering yield (shown by dashed line) is almost 20 times smaller than the observed one irrespective of the ion species and energy. This discrepancy may be attributed to the reduction of the surface binding energy caused by the high density of excitation and ionization along the ion path [4, 14]. Taking account of such an effect, the sputtering yields were calculated with lowered sublimation energies. The results were shown by solid lines in Fig. 5. With decreasing sublimation energy the calculated sputtering yield increases and the best fit to the observed result was obtained with U = 0.94 eV (shown by a thick solid line). The agreement with the observed result is reasonably good. It should be noted that U = 0.94 eV is, however, unrealistically small compared to the boiling energy (E_b = 2.5 eV [12]). Moreover, if we look at the partial sputtering yields, there is a large difference between the observed and calculated results.

Figure 6 shows the comparison between the observed and calculated partial sputtering yields. The circles show the observed result and the dashed lines show the calculated result for U = 0.94 eV. At lower C_{60} energies, the agreement is rather good. With increasing energy, however, the present calculation underestimates Y_N and overestimates Y_{Si}. Because the sublimation energies for Si and N are not necessarily the same, the partial sputtering yields Y_{Si} and Y_N were separately calculated with different

sublimation energies to see if the agreement is improved or not. The best fit results were obtained with U_{Si} = 1.04 eV and U_N = 0.91 eV for Y_{Si} and Y_N, respectively. The results are shown by solid lines in Fig. 6. The agreement is slightly improved but there are still rather large differences. The discrepancy can be more clearly seen by comparing the sputtering yield ratio Y_N/Y_{Si} as is shown in Fig. 7. The observed ratio increases with the energy of C_{60} and even larger for 100 MeV Xe. On the contrary, the calculated yield ratio is almost constant, showing that the observed preferential sputtering cannot be explained by the u-TS based calculation.

Figure 8 shows the observed yield ratio, Y_N/Y_{Si}, as a function of the fraction of the electronic energy loss $S_e/(S_e + S_n)$. All data points, including the result of 100 MeV Xe, follow one universal curve. At smaller S_e fractions, where the collisional sputtering is dominant, the observed yield ratio asymptotically approaches ~1.3. In the frame work of collisional sputtering, the sputtering yield ratio is given by [15]

$$\frac{Y_i}{Y_j} = \frac{c_i}{c_j}\left(\frac{M_j}{M_i}\right)^{2m}\left(\frac{U_j}{U_i}\right)^{1-2m}, \qquad (7)$$

where $c_{i,j}$ are the concentration of i and j species and m denotes the power exponent of the interaction potential. Using m = 0.19 [15] and $U_{Si} = U_N$, Eq. (7) predicts Y_N/Y_{Si} = 1.36. This is in good agreement with the observed asymptotic value at small S_e fractions (see Fig. 8). With increasing S_e fraction, however, the observed ratio deviates from Eq. (7) and asymptotically approaches ~9. This indicates that the observed large ratio, *i.e.* large preferentiality of nitrogen sputtering, is attributed to the electronic sputtering although the u-TS model cannot reproduce the observed large preferentiality. In addition, the observed large sputtering yield also cannot be explained by the u-TS model as was discussed above. These results suggest that there is an additional sputtering mechanism of the electronic sputtering other than the thermal spike mechanism.

Similar large sputtering yields (~10^4 atoms/ion) were observed for LiF bombarded by swift heavy ions [4]. The observed huge sputtering yield of LiF was reproduced by the i-TS calculation with a substantially reduced sublimation energy of 1.3 eV (cf. the sublimation energy of LiF is 2.8 eV). The strong reduction of the sublimation energy was

suggested to be linked to the emission of cluster. This, however, cannot explain the present result because the cluster emission lead to stoichiometric sputtering [4].

As was mentioned in the section 3, the nitrogen depletion occurs in the surface region down to ~ 15 nm in the case of the 540 keV C_{60} irradiation (see Fig. 2). The TEM observation showed that 540 keV C_{60} ions produce continuous ion tracks in a-SiN. The observed core radius was ~2 nm and the track length was ~15 nm [12, 16]. This track length coincides with the nitrogen depletion depth observed by RBS in the present study. Using high-angle annular dark field scanning transmission electron microscopy (HAADF-STEM), the density distribution around the track center can be derived [17]. From the density profile, the number of the atoms removed from the track core was estimated to be ~3600 [18]. Considering the semi-quantitative nature of the HAADF-STEM analysis, the estimated number is in good agreement with the measured sputtering yield (5020 ± 450). These results indicate that the sputtered atoms are emitted from the track core (radius ~ 2 nm and length ~ 15 nm) in the case of 540 keV C_{60} irradiation. Recalling that the track core is formed in the region where the temperature surpass the boiling energy, the additional mechanism might be a kind of gas-flow mechanism [19, 20]. It is noteworthy that nitrogen depletion caused by electronic excitations were also observed for various nitride films [21 – 24]. In these studies, the molecular recombination model was often used to explain the observed nitrogen depletion. In view of these studies, the preferential sputtering of nitrogen observed in the present work could be explained by the gas-flow of recombined nitrogen molecules.

V. CONCLUSION

The sputtering yield of amorphous silicon nitride irradiated with 30 – 1080 keV C_{60} and 100 MeV Xe ions were measured using high-resolution RBS. The results of the measurement showed that there is a synergy effect between the collisional and electronic sputtering. Large preferential sputtering of nitrogen was also observed especially at higher energies. The sputtering yields were calculated based on the u-TS model, which includes contributions of the elastic-collision spike, the inelastic thermal spike and the synergy effect.

The sputtering yields calculated with the sublimation energy of 2.5 eV were much smaller than the observed results, especially in the high energy region where the electronic energy loss is dominant. The agreement was improved if a reduced sublimation energy was used. The observed large preferential sputtering of nitrogen, however, could not be explained by the u-TS based calculation even if different sublimation energies were used for Si and N. The present results suggest that there is an additional sputtering mechanism related to the electronic energy loss. A possible mechanism might be a kind of gas-flow mechanism associated with decomposition of a-SiN induced by electronic excitations.

Acknowledgement

This work was performed under the shared use program of JAEA facilities. The authors are grateful to the crews of the 400-kV ion implanter at JAEA/Takasaki for irradiation of C_{60} ions. They are also grateful to the technical staff of the accelerator facilities at JAEA/Tokai for the irradiation of Xe ions. This work was partly supported by JSPS KAKENHI Grant (Grant Numbers 24651114 and 26246025).

References

[1] P. Sigmund, Phys. Rev. **184**, 383 (1969), P. Sigmund: in R. Behrisch (Ed.): *Sputtering by Particle Bombardment I*, Top. Appl. Phys. **47** (Springer, Berlin, Heidelberg 1981) p. 9.

[2] W. Assmann, M. Toulemonde, and C. Trautmann, in *Sputtering by particle Bomberdment, Topics Appl. Physics* **110**, Eds. R. Behrisch and W. Ekstein (Springer-Verlag, Berlin Heidelberg, 2007) p.401.

[3] M. Toulemonde, W. Assmann, C. Dufour, A. Meftah, F. Studer, and C. Trautmann, Mat. Fys. Medd. **52** (2006) 263.

[4] M. Toulemonde, W. Assmann, C. Trautmann, and F. Grüner, Phys. Rev. Lett. **88** (2002) 057602.

[5] K. Kimura, S. Joumori, Y. Oota, K. Nakajima, and M. Suzuki, Nucl. Instr. and Methods in Phys. Res. B **219-220** (2004) 351.

[6] J.F. Ziegler, J.P. Biersack, U.L. Littmark, The Stopping and Range of Ions in Solids,

Pergamon Press, New York, 1985.

[7] P.K. Haff, Appl. Phys. Lett. **29** (1976) 473.

[8] N. Matsunami, O. Fukuoka, T. Shimura, M. Sataka, S. Okayasu, Nucl. Instrum. Methods Phys. Res., Sect. B **230** (2005) 507.

[9] M. Toulemonde, W.J. Weber, G. Li, V. Shutthanandan, P. Kluth, T. Yang, Y. Wang and Y. Zhang, Phys. Rev. B **83** (2011) 054106.

[10] P. Kluth, C. S. Schnohr, O. H. Pakarinen, F. Djurabekova, D. J. Sprouster, R. Giulian, M. C. Ridgway, A. P. Byrne, C. Trautmann, D. J. Cookson, K. Nordlund, and M. Toulemonde, Phys. Rev. Lett. **101** (2008) 175503.

[11] M. Toulemonde, A. Benyagoub, C. Trautmann, N. Khalfaoui, M. Boccanfuso, C. Dufour, F. Gourbilleau, J. J. Grob, J. P. Stoquert, J. M. Costantini, F. Haas, E. Jacquet, K.-O. Voss, and A. Meftah, Phys. Rev. B **85** (2012) 054112.

[12] T. Kitayama, Y. Morita, K. Nakajima, K. Narumi, Y. Saitoh, M. Matsuda, M. Sataka, M. Tsujimoto, S. Isoda, M. Toulemonde, and K. Kimura, Nucl. Instr. and Methods in Phys. Res. B **356-357** (2015) 22.

[13] P. Sigmund and C. Claussen, J. Appl. Phys. **52** (1981) 990.

[14] C. C. Watson and T. A. Tombrello, Radiat. Eff. **89** (1985) 263.

[15] H. Gades, H. M. Urbassek: Nucl. Instrum. Methods Phys. Res., Sect. B **102** (1995) 261.

[16] Y. Morita, K. Nakajima, M. Suzuki, K. Narumi, Y. Saitoh, N. Ishikawa, K. Hojou, M. Tsujimoto, S. Isoda, and K. Kimura, Nucl. Instrum. Methods Phys. Res., Sect. B **315** (2013) 142.

[17] K. Nakajima, Y. Morita, M. Suzuki, K. Narumi, Y. Saitoh, N. Ishikawa, K. Hojou, M. Tsujimoto, S. Isoda and K. Kimura, Nucl. Instrum. Methods Phys. Res., Sect. B **291** (2012) 12.

[18] K. Nakajima, Y. Morita, T. Kitayama, M. Suzuki, K. Narumi, Y. Saitoh, M. Tsujimoto, S. Isoda, Y. Fujii and K. Kimura, Nucl. Instrum. Methods Phys. Res., Sect. B **332** (2014) 117.

[19] H. M. Urbassek and J. Michil, Nucl. Instrum. Methods Phys. Res., Sect. B **22** (1987) 480.

[20] M.M. Jakas, E.M. Bringa, and R.E. Johnson, Phys. Rev. B **65** (2002) 165425.

[21] S. R. Walker, J. A. Davies, J. S. Forster, S. G. Wallace and A. C. Kockelkoren, Nucl. Instrum. Methods Phys. Res., Sect. B **136** (1998) 707.

[22] K. Kimura, K. Nakajima, H. Kobayashi, S. Miwa and K. Satori, Nucl. Instrum. Methods Phys. Res., Sect. B **190** (2002) 423.

[23] S. K. Shrestha, K. Scott, A. Butcher, M. Wintrebert-Fouquet and H. Timmers, Nucl. Instrum. Methods Phys. Res., Sect. B **219** (2004) 686.

[24] N. Gordillo, R. Gonzalez-Arrabal, A. Rivera, F. Munnik and F. Agulló-López, Nucl. Instrum. Methods Phys. Res., Sect. B **289** (2012) 74.

Figure captions

Fig. 1 Observed <111> channeling (solid line) and random (dashed line) spectra of the pristine a-SiN/Si(001). The spectra observed after irradiation with 540 keV C_{60} ions to a fluence of 5.2×10^{12} ions/cm^2 are shown by symbols.

Fig. 2 Composition depth profiles of the pristine a-SiN/Si(001) derived from the observed high-resolution RBS spectra (open symbols). The profiles observed after irradiation with 540 keV C_{60} ions to a fluence of 5.2×10^{12} ions/cm^2 are shown by solid symbols.

Fig. 3 Areal density of Si in the a-SiN film as a function of the ion fluence. The dashed lines show the results of exponential fitting.

Fig. 4 Areal density of N in the a-SiN film as a function of the ion fluence. The dashed lines show the results of exponential fitting.

Fig. 5 Observed total sputtering yield as a function of C_{60} ion energy. The result of 100 MeV Xe ions is also shown for comparison. The lines show the results of the u-TS calculation for various sublimation energies. The best fit result is obtained with U = 0.94 eV (thick solid line).

Fig. 6 The observed partial sputtering yields of Si and N as functions of C_{60} ion energy. The result of 100 MeV Xe ions is also shown for comparison. The dashed lines show the u-TS results calculated with U = 0.94 eV. The solid lines show the best fit results calculated with different sublimation energies for each element.

Fig. 7 The sputtering yield ratio Y_N/Y_{Si} as a function of C_{60} ion energy. The result of 100 MeV Xe ions is also shown for comparison. The dashed line is drawn to guide the eye. The solid line shows the u-TS result with sublimation energies U_{Si} = 0.91 eV and U_N = 1.04 eV. The u-TS calculation cannot reproduce the observed preferential sputtering of nitrogen.

Fig. 8 The sputtering yield ratio Y_N/Y_{Si} as a function of the fraction of the electronic stopping power $S_e/(S_e + S_n)$. The dashed line is drawn to guide the eye. With increasing S_e fraction, the sputtering yield ratio increases from ~1.3 to ~9.

Table 1 Observed sputtering yields and collisional sputtering yields calculated using the SRIM code. The energy losses calculated using SRIM are also shown.

	Sputtering Yield (atoms/ion)					Energy Loss (keV/nm)	
	Y_{Si}	Y_N	Y_{total}	Y_{SRIM}	Y_N / Y_{Si}	S_n	S_e
30 keV C_{60}	540 ± 90	660 ±100	1200 ± 140	70	1.4 ± 0.2	8.27	1.71
120 keV C_{60}	1160 ± 130	1840 ± 200	3000 ± 240	82	1.9 ± 0.2	10.34	3.41
540 keV C_{60}	1510 ± 210	3510 ± 390	5020 ± 450	66	3.4 ± 0.4	9.55	7.24
1080 keV C_{60}	810 ± 170	3790 ± 450	4590 ± 480	56	4.2 ± 0.6	7.98	10.24
100 MeV Xe	46 ± 190	410 ± 190	460 ± 270	0.27	8.9 ± 26	0.12	16.43

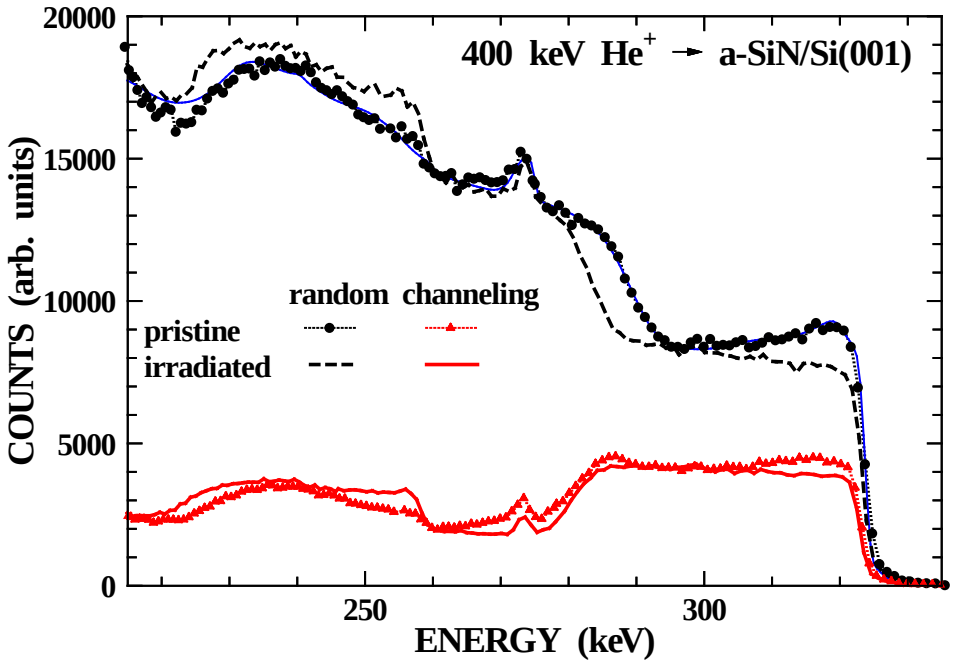

Fig. 1

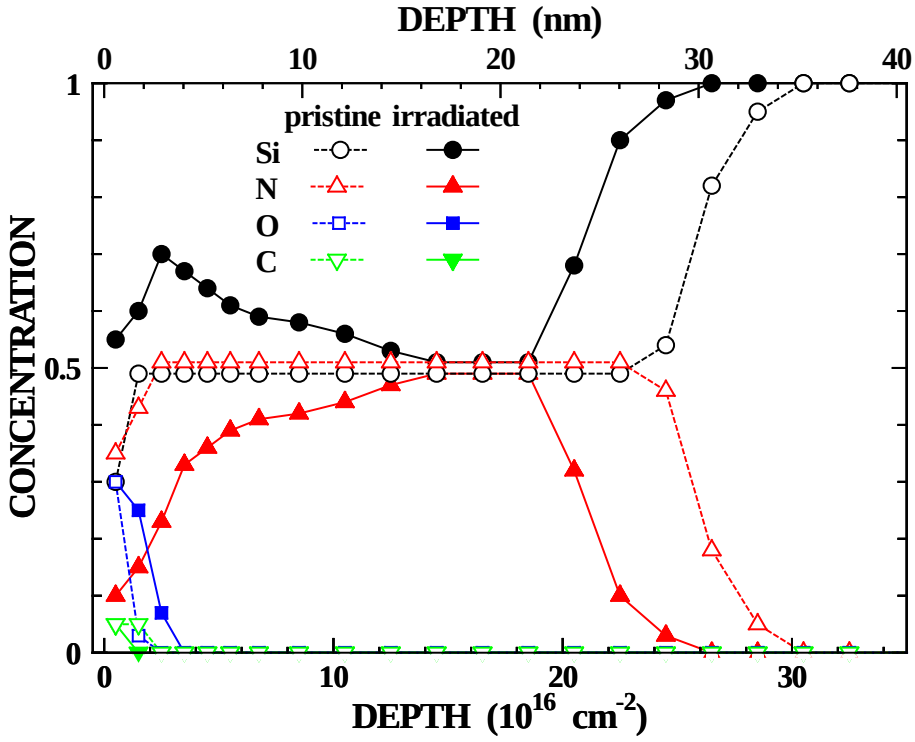

Fig. 2

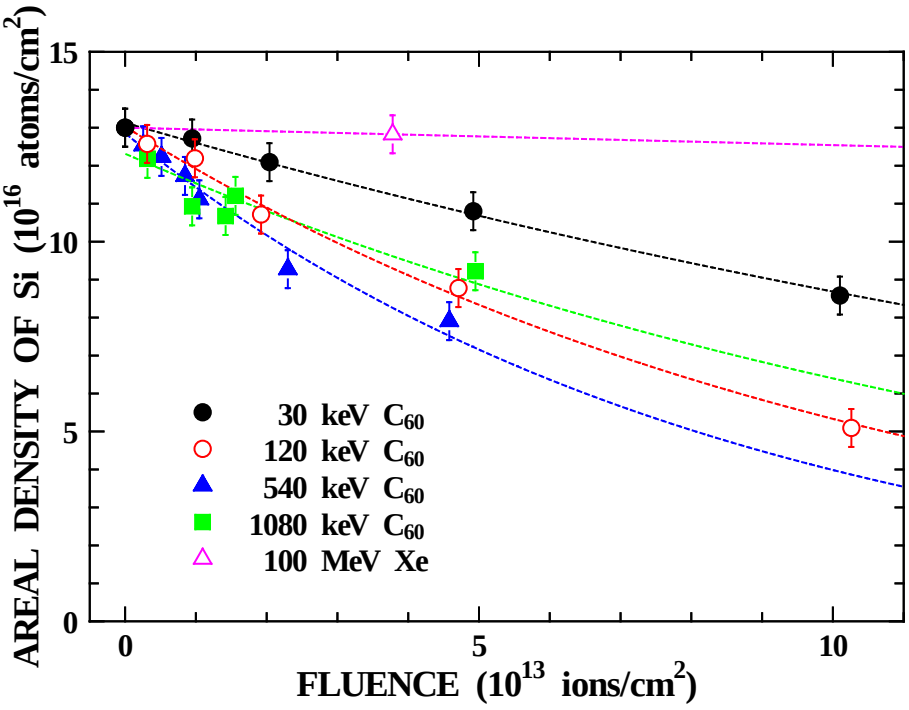

Fig. 3

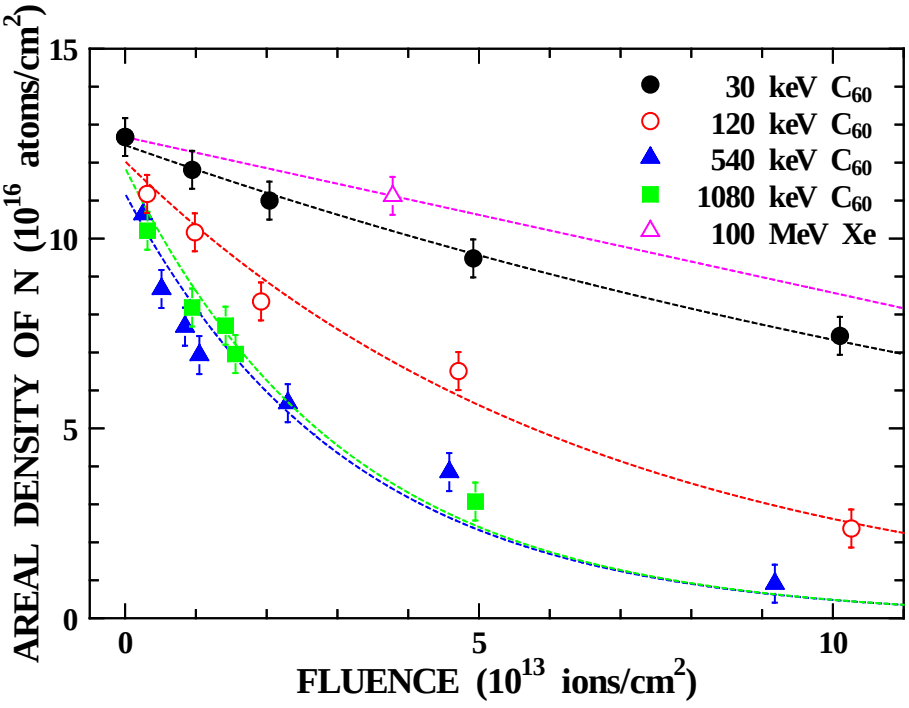

Fig. 4

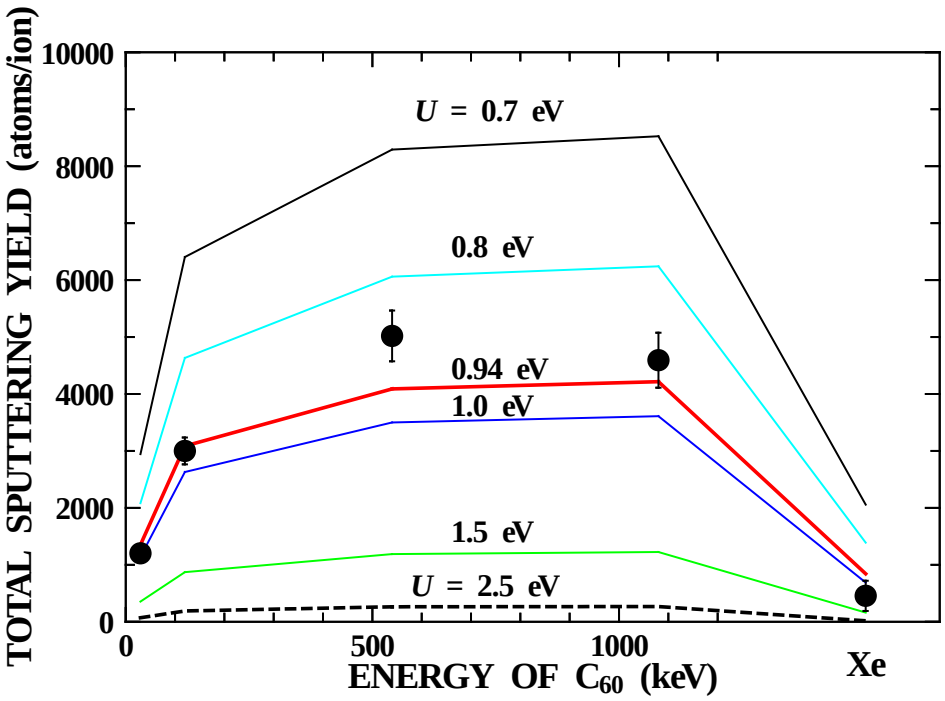

Fig. 5

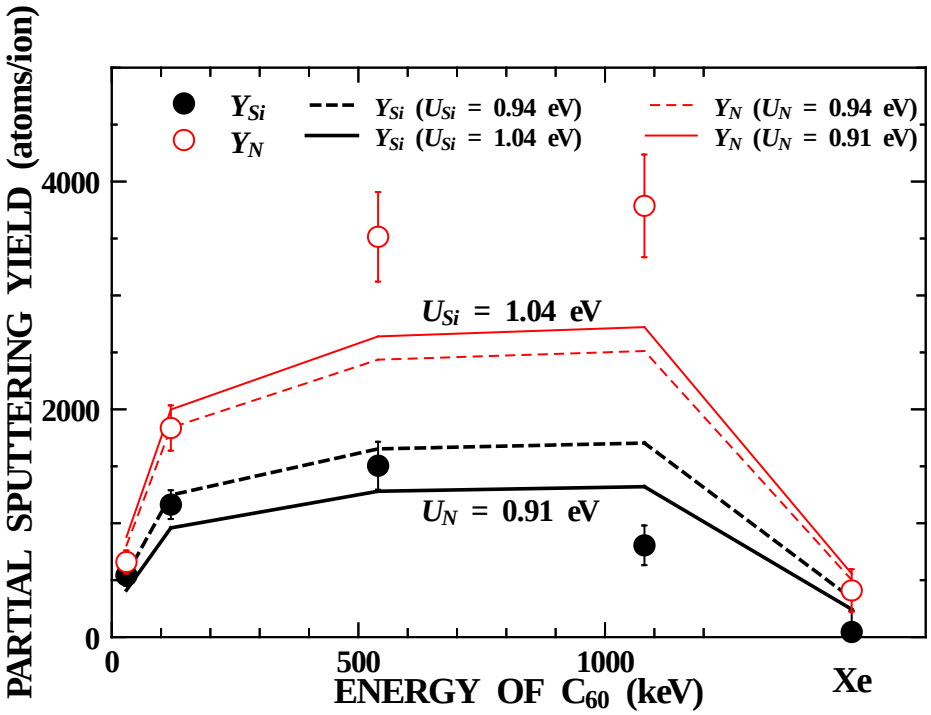

Fig. 6

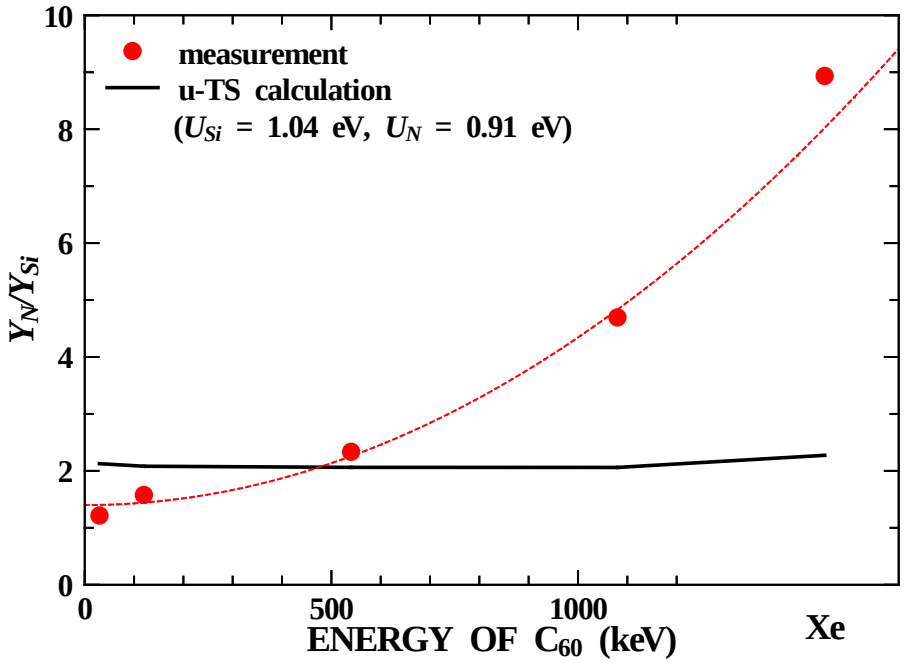

Fig. 7

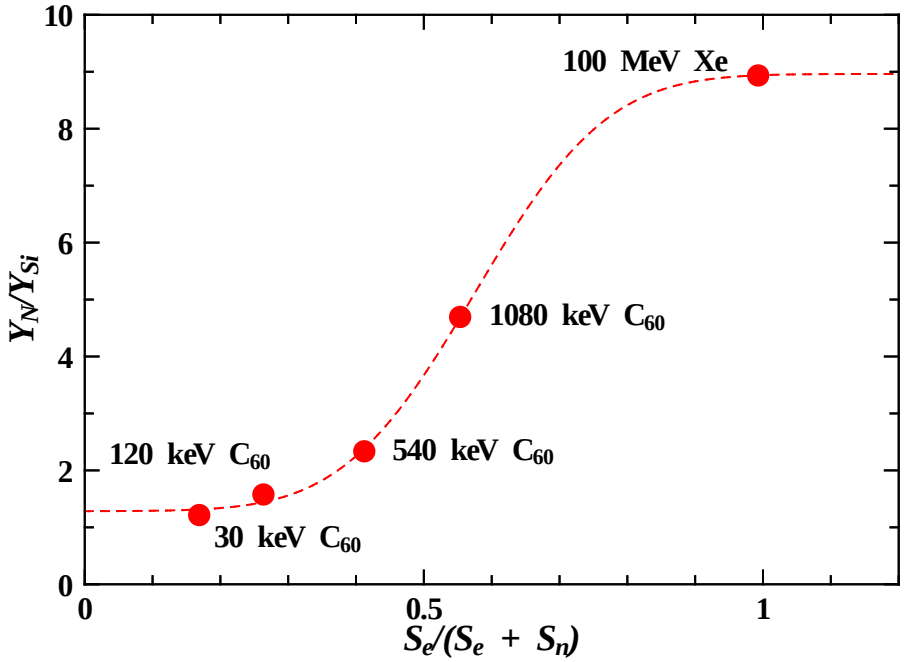

Fig. 8